Full Paper
Journal of Nano Materials Impact 2025, 01 (02) 10-16

Employ ZnO/NiO Nanocomposites as Catalyst for Photo Degradation of Methylene Orange Dye in Water

Hejran Qais Faris, Radhiyah M. Aljarrah*
Department of Physics, Faculty of Science, University of Kufa, Nagaf, IRAQ.

Abstract
This work attempts to enhance the photocatalytic activity of methylene orange by adding X% ZnO/NiO nanoparticles. For this purpose, zinc oxide and nickel oxide nanoparticles and nanocomposites have been prepared (where X: 100, 75, 50, 25, and 0%). The structural properties of the prepared nanomaterials were studied using XRD, FESEM, and EDX. The result revealed that the particle distribution was homogeneous, with overlap between the hexagonal zinc oxide and cubic nickel oxide lattices. On the other hand, the energy band gap of the prepared samples was determined using UV-Vis diffuse reflectance spectroscopy. The performance of ZnO and NiO particles and their nanocomposites in the photodegradation of methylene orange (MeO) dye was evaluated using UV light as a catalyst. The photocatalytic efficiency was determined through the photodegradation of MeO dye. The results show that the ZnO/NiO nanocomposites give a good photodegradation rate. The results show that the peak degradation of the dye is at the wavelength of 465 nm, and the highest photodegradation efficiency is 76% for the Zn-25% nanocomposites after 180 minutes of irradiation.

Keyword: hydrothermal process • methylene orange • nanocomposites • photocatalytic.

Introduction

Recently, Water pollution with harmful substances such as chemicals or pathogens has been considered one of the main sources of environmental pollution. Release this contaminated water without treatment to nature, its negative impact will extend; the impact is not limited to polluting the water but extends to aquatic ecosystems[1]. Organic Dyes are the main contaminant element in industrial wastewater, due to their widespread use in industries such as textiles, leather, paper, and plastics. Unfortunately, these dyes have a complex chemical composition, which makes them resistant the degradation by conventional wastewater treatment processes[2-4]. Therefore, the conventional wastewater treatment methods often struggle to effectively remove persistent organic pollutants such as dyes. To address this issue, researchers attempt to explore an advanced materials and technologies could offer a reasonable solution. Photo degradation processes it is one of the techniques that employ metal oxides as catalysts to stimulate and accelerate the interaction. Zinc oxide (ZnO), titanium dioxide (TiO_2), and nickel oxide (NiO) possess properties that make them able to catalyze the reaction, and can employ them to be highly effective in environmental remediation[5-8].

***Address for correspondence:** Radhiyah M. Aljarrah, Department of Physics, Faculty of Science, University of Kufa/ Nagaf, Iraq.
E-mail: radhiyah.aljarrah@uokufa.edu.iq
ORCID: https://orcid.org/0000-0003-3431-4238

Info:
Submitted: 08 Feb. 2025; **Revised:** 25 March 2025;
Accepted: 21 April 2025; **Published:** 18 Aug. 2025.
https://doi.org/10.71109/nmi.2025.1.2.11

Zinc oxide is of interest to researchers in this field because it has a strong photocatalytic activity under UV light, and it provides oxygen species such as hydroxyl radicals when exposed to UV light, which then react with organic pollutants such as dyes and degrade them into less harmful compounds[9-12]. In addition, it is inexpensive and non-toxic[13, 14]. Nickel oxide's importance is due to its ability to catalyze the oxidation of organic compounds[15]. Also, the magnetic properties of NiO enable it to be easily recollected after utilization, making it a reusable and sustainable option for wastewater treatment. Therefore, a combination of different metal oxides, such as ZnO/NiO nanocomposites, has shown synergistic effects that enhance the photocatalytic performance and allow for more efficient degradation of pollutants[16]. Hence, the motivation of this work is it focus on preparing a mix of nanoparticles of zinc and nickel oxides in different weight ratios in order to employ them to purify water from toxic organic compounds. In this study, the hydrothermal method was used to prepare nanomaterials because it has many advantages over other growth processes, such as the use of simple equipment, catalyst-free growth, low cost, uniform production over a large area, environmental friendliness, and low risk.

Experimental Part

Preparation of Nanomaterials via Hydrothermal Method

In this research, the hydrothermal method was used to prepare nanoparticles of zinc oxide, nickel oxide, and their compounds.

To determine the molarity concentration using the equation[17]:

$$M = \frac{W_t}{M_{wt} \times \frac{V}{1000}} \quad \text{... (1)}$$

where M is the molar concentration, W_t is the weight of material, *Mwt*: Molecular weight, and V: volume of distilled water. To prepare zinc oxide nanoparticles (NPs) a 3 g of zinc acetate $Zn(Ch_3COO)_2•2H_2O$ salt was dissolved in 75 ml of deionized water and stirred for 1 hour. Sodium hydroxide solution (was prepared by dissolving 1.5 g of NaOH in 75 ml of deionized water and stirring for 30 min) was mixed gradually until the color of the resulting solution began to be milky, followed by stirring for 1h.

A 100 ml of the results mixing was taken to a Teflon-lined stainless-steel autoclave (100ml), and heated using an oven at 140 °C for 5 hours, then cooled to room temperature. Precipitate white powder has been deposited. The resulting powder was extracted, washed using distilled water and ethanol several times, and dried by centrifuge at 5500 rpm, then used oven sated at 80 °C. The dried powder was annealed at 400 °C for 2 hours. The calcination process has improved the crystallinity of the nanoparticles, which has resulted in enhanced photocatalytic activity and optical properties[6]. Using the same steps, nickel oxide can be prepared using 3 g of nickel nitrate salt $Ni(NO_3)_2$ dissolved in 75 ml of deionized water. To synthesize ZnO/NiO nanocomposites (NCs) (75% ZnO/25% NiO denoted by ZN-25), ZN-50, and ZN-75, using the hydrothermal technique. The three samples of nanocomposite (NCs) have been prepared by dissolving $Zn(Ch_3COO)_2•2H_2O$ /$Ni(NO_3)_2$, 2.25/0.75, 1.5/1.5, and 0.25/2.75g) in 75 ml of deionized water. Follow that by adding NaOH (0.5 M) and stirring it for one hour. The solutions were subjected to heat treatment by being heated to 140 °C for 5 hours, then left to cool gradually to room temperature. Then, the same steps were followed in preparing the nanoparticles of zinc and nickel oxide. FESEM model TESCAN - (MIRA3, LMU) was used to characterize the surface morphology, a high magnification of 100.0 kx was used to illustrate the nanostructure, with an accelerating voltage of 20.0 kV and a working distance of 7.29 mm. For photocatalytic measurements, a 15 ppm (part per million) solution of methylene orange dye was prepared, and UV light (Xenon lamp, 240 W, 365 nm wavelength) was used.

Results and Discussion

X-Ray Diffraction Analysis

The structural and compositional properties of the prepared nanomaterials were determined by X-ray diffraction (using a Philips X-ray diffraction system, the radiation source is Cu (kα) and the wavelength λ = 1.5406, the current is 30 mA, and the voltage is 40 kV). The intensity was recorded versus Bragg diffraction angle in the range (20°-80°).

The X-ray diffraction data were recorded and compared with the standard cards for ZnO and NiO materials, where they were in full agreement with the standard ZnO JCPDS No. 76-0704 and NiO JCPDS No. 00-047-1049[18].

The broadening of the peaks in the diffraction pattern is an indication that the synthesized materials are within the nanometer scale. From **Figure 1**, the diffraction peaks of hexagonal ZnO appear at angles (31.7, 34.4, 36.2, 47.5, 56.6, 62.9, 66.4, 68, 69.3, 72.6, and 77.1) corresponding to the (100), (002), (102), (110), (103), (112), and (004) planes. When NiO is added at a rate of 25%, the ZnO peaks clearly appear at the same positions as (100) and (002), but they are less intense compared to pure ZnO, as the face-centered cubic NiO begins to overlap with the hexagonal ZnO crystal lattice. When NiO concentration increased by 50%, new peaks appeared at angles of 37.1° and 43.2°, corresponding to the (101) and (200) planes where the NiO particles are concentrated. A further decrease in the intensity of the main zinc oxide peaks (e.g., the (100) and (002) planes) was observed. This pattern indicates significant overlap between the NiO and ZnO, leading to a rearrangement of the crystal lattice and possibly the formation of a mixed phase between the two materials. When the nickel oxide concentration was increased to 75%, additional peaks appeared compared to the main NiO peaks.

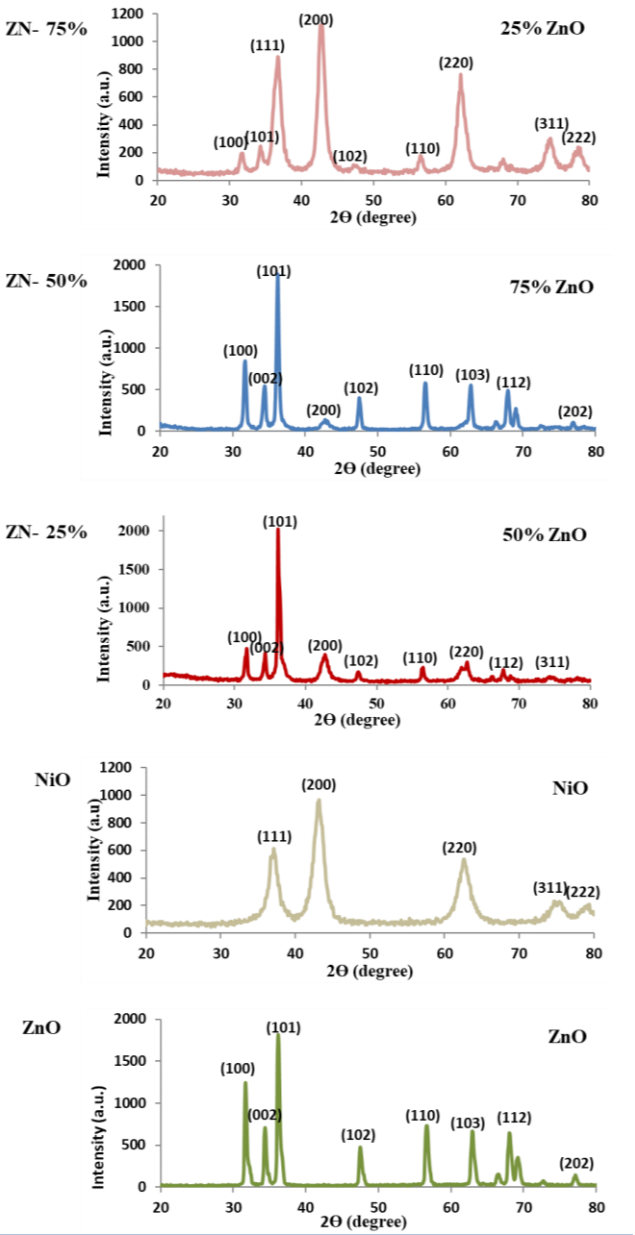

Figure 1. XRD patterns of ZnO/NiO NPs and NCs at different concentrations.

These peaks are due to the hexagonal wurtzite crystal structure that characterizes ZnO. This indicates that ZnO

added a new dimension to the crystal structure, either through the formation of a new phase resulting from the interaction between the two materials during heat treatment, or through the growth of discrete zinc oxide crystals within the nickel oxide lattice. The results are consistent with[19].

The average crystallite size of the samples was estimated with the help of Scherer equation:

$$D = 0.9\lambda/(\beta \cos\theta) \quad \ldots (2)$$

In this equation, λ is the wavelength of X-ray (1.5406 Å), β is the full width of the half-maximum (FWHM) in rad, and θ is the Bragg diffraction angle.

The average crystal size of the prepared nanomaterials was found in the range between 21-30 nm, depending on the percentages of the materials entering the composition. This result indicates that the size of the prepared particles falls within the nanoscale. The quality of the prepared nanomaterials is mainly affected by the reaction conditions, such as temperature and processing time. As the NiO concentrations increase, FWHM increases, thus the size of nanoparticles decreases. This is due to the change in growth rate between the different crystal lattices. **Table 1** shows the value of the average nanoparticle size. The results are consistent with[20, 21].

Table 1. The average crystalline size of ZnO/NiO nanocomposites.

Compositions	Average of Crystalline size(nm)
ZnO	ZnO
ZN-25%	ZN-25%
ZN-50%	ZN-50%
ZN-75%	ZN-75%
NiO	NiO

FESEM and EDX Analysis

The X-ray diffraction results indicate that the introduction of ZnO in different proportions clearly affected the crystal structure, resulting in the emergence of new properties due to the overlap between the crystal structures of NiO and ZnO. However, to understand the nature of the resulting phases more precisely, it will be necessary to conduct additional analyses using techniques such as electron microscopy to examine the crystal and microstructure, and EDX analysis to study the chemical composition and element distribution.

The FESEM image in **Figure 2** shows the nanostructure properties of a hydrothermally prepared ZnO, NiO, and their composites. The nanoparticles are distributed on the surface of the sample in a relatively uniform manner, with a clear contrast in the particle size, with from 11 nm to 25 nm. The variation in the size may be the result of the conditions of thermal preparation, such as the temperature and the treatment time, in addition to the concentration of the ingredients of the samples of zinc and nickel oxides. The presence of nickel oxide acted as an inhibitor of the growth of zinc oxide particles and vice versa, which contributed to obtaining small and similar sizes, and was the lowest value of the particle size of the concentration ZN-25% as shown in **Table 2**. It changes with the change of the concentrations, and the shape of the grenades was in the form of rice particles for the nickel oxide sample. As for the rest of the samples, the shape of the particles was spherical.

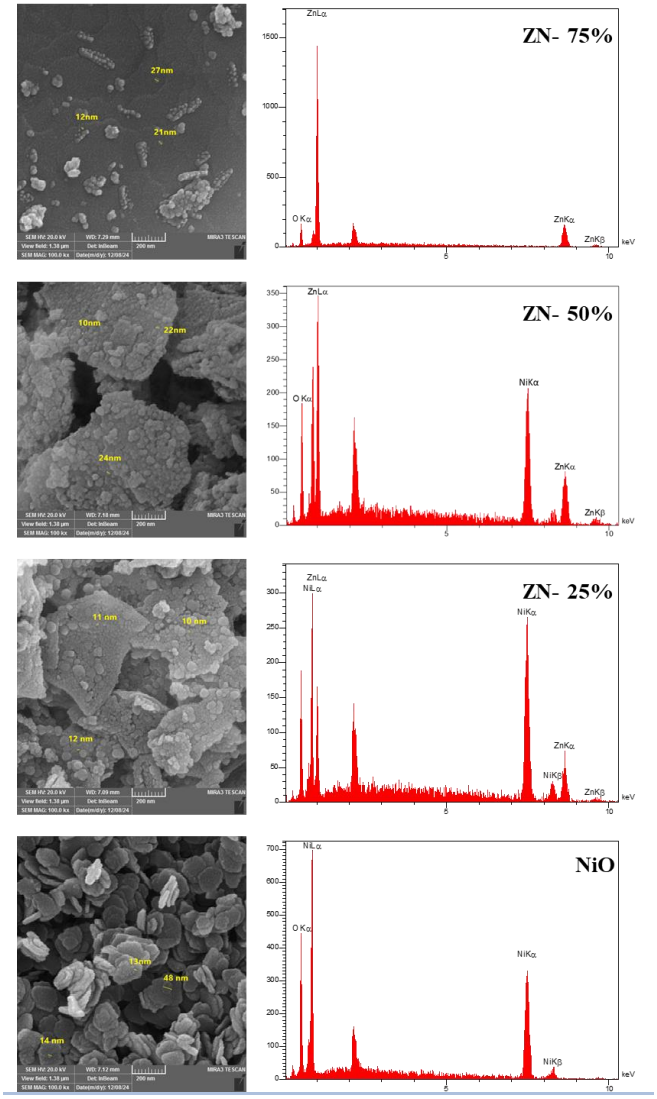

Figure 2. FESEM images and EDX of ZnO/NiO NPs at different concentrations and NiO NPs.

The aggregate elemental composition of the phases in the sample is determined using EDX attached to the SEM instrument, as in Figure 2. EDX spectra of ZnO/NiO nanoparticles deposited with various concentrations, which confirm the existence of elements (zinc, nickel, and Oxygen), constitute the nanoparticles' structure. The figures are showing a good sample stoichiometry. The zinc, nickel, and oxygen peaks appear as indicated in the figure, and there is a peak associated with the substrate used, a clear peak in the center, not indicated in all the EDX spectra.

Table 2. The average grain size of ZnO/NiO nanocomposites and NiO NPs.

Compositions	Average of grain size (nm)
ZnO	20
ZN-25%	18
ZN-50%	14
ZN-75%	11
NiO	25

Diffuse Reflectance Spectroscopy Measurements (DRS)

The optical properties of a pure ZnO and NiO metal oxides nanoparticles and ZnO/NiO heterostructured compounds with different ratios (25/75, 50/50, and 25/75%) were studied using UV-Vis diffuse reflectance spectroscopy (DRS) in the wavelength range of 200 to 800 nm; **Figure 3.** shows the energy gap values of the prepared nanomaterials, where the band gap of the nanomaterial was found from the modified Kubelka-Munk (K-M) function plots. The reflectance (R) data is correlated with the absorption coefficient (α) according to the Kubelka-Munk function in the following manner[22]:

$$F(R) = \frac{(1-R)^2}{2R} = \frac{\alpha}{S} \quad \ldots (3)$$

Where α and S are the absorption and scattering K-M coefficients, respectively. And the K-M function can be written as follows[23-26]:

$$[F(R)h\nu]^n = (\alpha h\nu)^n = B\left(h\nu - E_g\right) \quad \ldots (4)$$

Here, Eg is the optical energy gap, hν is the incident photon energy, and n is a constant that varies according to the optical transition. The reflectance (R) data shown as F(R) were obtained by introducing the K-M algorithm[11]. In the UV, visible diffuse reflectance absorption spectra, the plot of $[F(R)h\nu]^n$ versus incident photon energy hν indicates that the optical transitions are direct, and the band gap can be found by extrapolating the linear part of the curve along its straight line and the section on the energy axis indicates the value of the energy gap.

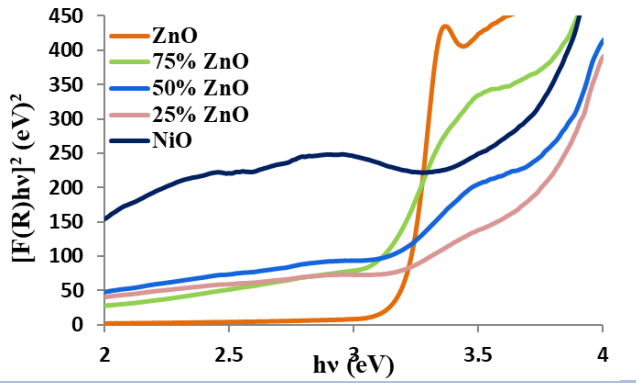

Figure 3. Kubelka-Munk plot to find Eg of ZnO/NiO nanocomposites and NiO NPs

From studying the obtained results, it can be observed that the energy gap changes with the change in the percentages of the nanocomposites as well as with the change in the shape and size of the nanomaterials[27]. It can be noted that for some samples, there are two energy gaps. It is important to mention that indirect transitions can occur simultaneously with direct transitions, but they cannot be detected in the absorption spectrum due to their high energy and low probability. The results are shown in **Table 3.** These results are in agreement with[20]. This significant increase in the optical band gap values of the ZnO/NiO nanocomposites with increasing NiO concentration is attributed to the effect of smaller particle size, which leads to band bending as the larger the surface to volume ratio of the nanoparticles, the greater the band bending effect[28]. Moreover, the increasing band gap values with smaller particle size of the samples indicate the quantum confinement effect of the ZnO/NiO nanocomposites[29].

Table 3. Eg values of various ZnO/NiO nanocomposites and NiO NPs.

Compositions	Eg (eV)
ZnO	3.2
ZN-25%	3.05- 3.15
ZN-50%	2.92 – 3.49
ZN-75%	3.34
NiO	3.53

Photocatalytic Measurements

In this work, (MeO) dye at a concentration of 15 ppm was used as a representative pollutant to determine the photocatalytic efficiency of this dye. The dye mixture was prepared by dissolving (0.1 g) of the dye in 100 ml of distilled water, and then 1.5 ml of this main solution was taken and diluted in 100 ml of distilled water to prepare a concentration of 15 ppm. The semiconductor dye mixture was prepared by dissolving 0.2 g of the catalyst nanomaterials (prepared) in the dye solution. After 30 min of mixing and stirring in the dark using a magnetic stirrer, the dye and catalyst reached the absorption equilibrium state. Then, the solution was illuminated using a UV source as an activator for the photocatalytic process, and the dye degradation was measured every 30 min for 180 min using a UV-Vis spectrometer.

The study was conducted to examine the impact of five distinct catalysts (ZnO, ZN-25%, ZN-50%, ZN-75%, and NiO) on the photocatalytic degradation efficiency of MeO dye. The experiments were conducted under identical conditions, including a concentration of MeO dye at 15 ppm, and exposure to UV light irradiation for 180 min to compare their performances.

The absorption spectra of the samples exposed to UV radiation were measured at separate time intervals (every 30 min) to obtain the amount of dye effect of the photocatalytic process of pure and mixed materials and to study the degradation rate which was calculated in terms of the change in intensity at the maximum at the wavelength of 465 nm for methylene orange (MeO) dye **Figure 4.** The decolorization efficiency of the sample was determined as a percentage from the following equation[30]:

$$Efficiency\% = \frac{C_o - C}{C_o} \times 100 \quad \ldots (5)$$

where C_o and C represent the concentration of the initial solution and concentration at different time intervals, respectively. After 30 minutes of exposure to UV radiation, pure methylene orange dissolved in water begins to decompose. The UV-light exposure process continues for 180 min during which the residual concentration of MeO dye in the overlying liquid is determined every 30 minutes by measuring its absorbance using UV-visible spectroscopy, as shown in **Figure 5.**

The type of catalyst showed a significant effect on the degradation rate. However, catalysts showed varying effects.

ZnO and NiO nanoparticles and their composites have been shown to be highly sensitive to UV radiation and act as good photocatalysts for removing pollutants from water.

In addition to the photocatalytic effect, the presence of a small amount of hydroxyl radical in water is also responsible for the decomposition of MeO.

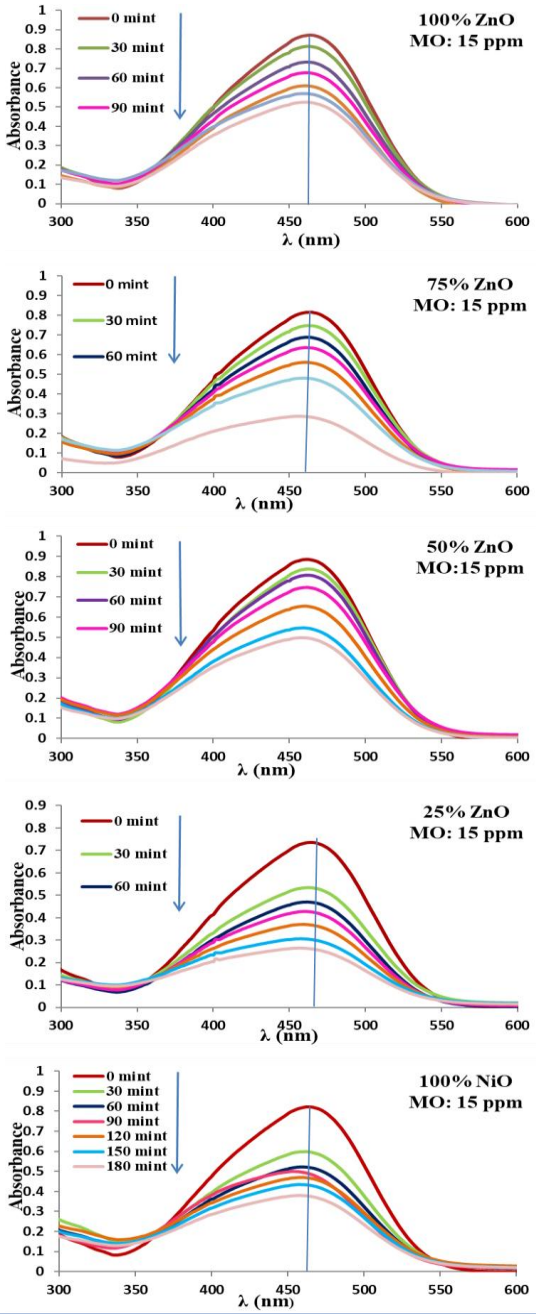

Figure 4. UV–Vis spectra of MeO degradation, versus irradiation time.

From the study of the obtained results, it was observed that the best photocatalytic degradation rate was found in ZN-75 nanocomposites, which is higher than that of ZnO and NiO. This enhanced photocatalytic activity of ZN-75 is attributed to the smaller particle size and increased surface area-to-volume ratio. This increased degradation rate is also attributed to improving the electrons and the holes generation efficiency and reducing recombination, which enhances the interaction of free radicals with the dye molecules. At low concentrations, the light absorption of the catalyst molecules is greater, allowing for the generation of a sufficient number of electrons and holes needed to produce hydroxyl free radicals ($^{*}OH$), holes (H^{+}), superoxide ions (O_2^{*-}), and peroxide radicals ($^{*}H_2O$) can be photo-oxidized by nanomaterials, which play a role in dye degradation[30, 31]. The result is consistent with[32].

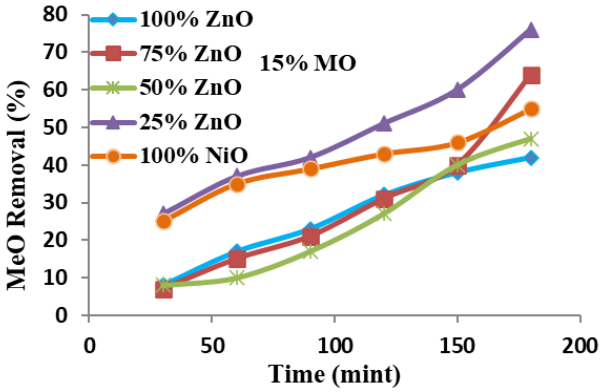

Figure 5. Effect of percentage of compositions (ZnO/NiO) on the degradation of MeO dye.

Table 4. Degradation percent (PDE) of MeO dye solutions with catalyst after 180 min under UV irradiation.

Compositions	PDE (%)
ZnO	42
ZN-25%	64
ZN-50%	47
ZN-75%	76
NiO	55

Conclusion

From this work, the following can be concluded: The XRD pattern shows two clear groups of diffraction peaks that correspond to hexagonal wurtzite of ZnO and face-centered cubic NiO. From the calculation of particle size of samples, it can be concluded that the ZnO/NiO NCs gave the sizes of the particles less than the ZnO and NiO NPs. On the other hand, UV-Vis diffuse reflectance spectroscopy results showed that mixing ZnO and NiO leads to changes in the band gap between 3.2 to 3.53 eV, which enhances of photocatalytic efficiency of ZnO/NiO nanocomposites. The best catalytic dose was obtained for different catalyst ratios of ZN-X% composites, for 15 ppm MeO dye. It was found that the highest degradation rate of this dye was for the nanocomposite at a concentration of ZN-75%, which gave the highest value for degradation efficiency of 76%. Thus, it can be concluded that ZnO and NiO nanocomposites can be used as photocatalysts for the photodegradation of aquatic and environmental pollutants

Acknowledgements

This work was carried out within the framework of treating the wastewater from factories that use organic dyes, such as textile factories and others. First, we thank the Physics Department at the University of Kufa, College of Science, for giving us the opportunity to work in the Thin Film Laboratory. We are also grateful to Professor Dr. Ali M. Al-

Joudah in the Physics Department, University of Babylon, College of Science, for his assistance in conducting the linguistic processing of the research

Declaration of Competing Interests

The authors declare that they have no conflicts of interest.

References

[1] K. Karthika and K. Ravichandran, "Tuning the Microstructural and Magnetic Properties of ZnO Nanopowders through the Simultaneous Doping of Mn and Ni for Biomedical Applications," *Journal of Materials Science & Technology*, vol. 31, no. 11, p. 1111-1117, 2015.

https://doi.org/10.1016/j.jmst.2015.09.001.

[2] F. Mohamadpour and A. M. Amani, "Photocatalytic systems: reactions, mechanism, and applications," *RSC Advances*, 10.1039/D4RA03259D vol. 14, no. 29, p. 20609-20645, 2024.

https://doi.org/10.1039/D4RA03259D.

[3] I. Rapti, V. Boti, T. Albanis, and I. Konstantinou, "Photocatalytic Degradation of Psychiatric Pharmaceuticals in Hospital WWTP Secondary Effluents Using g-C3N4 and g-C3N4/MoS2 Catalysts in Laboratory-Scale Pilot," *Catalysts*, vol. 13, no. 2,

https://doi.org/10.3390/catal13020252

[4] G. Patil, N. Bodawar, G. Khotari, P. Mulay, P. Khurpade, and S. Kamble, "Photocatalytic Degradation of Ciprofloxacin HCl using Visible Active BiOS Photocatalyst and Artificial radiation," *Journal of ISAS*, vol. 3, no. 2, p. 1-13, 2022.

https://doi.org/10.59143/isas.jisas.3.2.BTNT3094.

[5] V. Innocenzi, A. Colangeli, and M. Prisciandaro, "Advanced oxidation processes for the removal of dyes from synthetic industrial wastewaters," *Desalination and Water Treatment*, vol. 259, p. 315-320, 2022.

https://doi.org/10.5004/dwt.2022.28629.

[6] M. Hashim, M. Usman, S. Ahmad, R. Shah, A. Ali, and N. U. Rahman, "ZnO/NiO Nanocomposite with Enhanced Photocatalytic H2 Production," *International Journal of Photoenergy*, vol. 2024, no. 1, p. 2676368, 2024.

https://doi.org/10.1155/2024/2676368.

[7] C.-C. Hsu and N. L. Wu, "Synthesis and photocatalytic activity of ZnO/ZnO2 composite," *Journal of Photochemistry and Photobiology A: Chemistry*, vol. 172, no. 3, p. 269-274, 2005.

https://doi.org/10.1016/j.jphotochem.2004.12.014.

[8] A. Y. Al-Jumaily, S. S. Al-Jubori, and A. Al-Haddad, "Green synthesized TiO2 nanoparticles impact on extensive-drug resistance gram-negative bacteria," *AIP Conference Proceedings*, vol. 3097, no. 1, p. 020014, 2024.

https://doi.org/10.1063/5.0209550.

[9] D. L. Liao, C. A. Badour, and B. Q. Liao, "Preparation of nanosized TiO2/ZnO composite catalyst and its photocatalytic activity for degradation of methyl orange," *Journal of Photochemistry and Photobiology A: Chemistry*, vol. 194, no. 1, p. 11-19, 2008.

https://doi.org/10.1016/j.jphotochem.2007.07.008.

[10] R. Liu, Y. Huang, A. Xiao, and H. Liu, "Preparation and photocatalytic property of mesoporous ZnO/SnO2 composite nanofibers," *Journal of Alloys and Compounds*, vol. 503, no. 1, p. 103-110, 2010.

https://doi.org/10.1016/j.jallcom.2010.04.211.

[11] G. S. Sree, S. M. Botsa, B. J. M. Reddy, and K. V. B. Ranjitha, "Enhanced UV–Visible triggered photocatalytic degradation of Brilliant green by reduced graphene oxide based NiO and CuO ternary nanocomposite and their antimicrobial activity," *Arabian Journal of Chemistry*, vol. 13.

https://doi.org/10.1016/j.arabjc.2020.02.012.

[12] J. Li, Q. Wu, and J. Wu, "Synthesis of Nanoparticles via Solvothermal and Hydrothermal Methods," in *Handbook of Nanoparticles*, M. Aliofkhazraei, Ed. Cham: Springer International Publishing, 2016, pp. 295-328.

https://doi.org/10.1007/978-3-319-15338-4_17.

[13] R. Mou, Z. Liu, D. Zhang, and A. Yang, "Enhanced visible light induced photocatalytic degradation of oxytetracycline hydrochloride by n-ZnO/p-NiO composite," *Chemical Physics Letters*, vol. 829, p. 140741, 2023.

https://doi.org/10.1016/j.cplett.2023.140741.

[14] M. Yass, A. Al-Haddad, M. J. M. Ali, A. Jaafar, and M. Veres, "Effectiveness of Green Synthesized Zinc Oxide Nanoparticles against Extensively Drug-resistant Klebsiella pneumoniae," *Biomedical and Biotechnology Research Journal (BBRJ)*, vol. 7, no. 3, 2023.

https://doi.org/10.4103/bbrj.bbrj_167_23.

[15] H. H. Naseef, A. K. H. Albarazanchi, A. Al-Haddad, A. Jaafar, L. Himics, and M. Veres, "Innovative constructure of rGO/NiO nanosheet/nanopore arrays toward optical absorption enhancement via hybrid nanosurface," *Journal of Optics*, 2025.

https://doi.org/10.1007/s12596-025-02595-w.

[16] V. Selvaraj, T. Swarna Karthika, C. Mansiya, and M. Alagar, "An over review on recently developed techniques, mechanisms and intermediate involved in the advanced azo dye degradation for industrial applications," *Journal of Molecular Structure*, vol. 1224, p. 129195, 2021.

https://doi.org/10.1016/j.molstruc.2020.129195.

[17] R. M. Aljarrah and H. A. Hamza, "Effected of spraying solution concentration on SnO2 films properties for photo-detector application," *AIP Conference Proceedings*, vol. 2457, no. 1, p. 050011, 2023.

https://doi.org/10.1063/5.0118315.

[18] H. D. Weldekirstos, B. Habtewold, and D. M. Kabtamu, "Surfactant-Assisted Synthesis of NiO-ZnO and NiO-CuO Nanocomposites for Enhanced Photocatalytic Degradation of Methylene Blue Under UV Light Irradiation," (in English), *Frontiers in*

Materials, Original Research vol. Volume 9 - 2022, 2022.

https://doi.org/10.3389/fmats.2022.832439.

[19] K. Anandan, K. Rajesh, K. Gayathri, A. Rexalin Devaraj, M. Mohanbabu, and P. P. Rao, "Optical Properties of Heterostructured ZnO/NiO Nanocomposites Synthesized via Facile Precipitation Process," *Asian Journal of Chemistry*, vol. 35, no. 9, p. 2171-2175, 2023.

https://doi.org/10.14233/ajchem.2023.27794.

[20] L. Filipponi and D. Sutherland, *Nanotechnologies – Principles, applications, implications and hands-on activities (a compendium for educators)*. European Commission: Directorate-General for, Research Innovation,, 2012, p. 416.

https://doi.org/10.2777/76945.

[21] O. Stenzel, *The physics of thin film optical spectra: An introduction*, 2 ed. (Springer Series in Surface Sciences). Springer, 2016, p. 352.

https://doi.org/10.1007/978-3-319-21602-7.

[22] M. Fox, *Optical properties of solids*, 2 ed. Oxford university press, 2010.

[23] N. Khlifi, C. Zerrouki, N. Fourati, H. Guermazi, and S. Guermazi, "Investigation of structural and optical properties of TM-doped CuO NPs: Correlation with their photocatalytic efficiency in sunlight-induced pollutant degradation," *Measurement*, vol. 237, p. 115209, 2024.

https://doi.org/10.1016/j.measurement.2024.115209.

[24] G. G. Welegergs *et al.*, "Electrodeposition of nanostructured copper oxide (CuO) coatings as spectrally solar selective absorber: Structural, optical and electrical properties," *Infrared Physics & Technology*, vol. 133, p. 104820, 2023.

https://doi.org/10.1016/j.infrared.2023.104820.

[25] G. S. Varsha, R. Pavithran, and R. J. Bose, "Aqueous synthesis of bare and Ag incorporated ZnO, CuO and ZnO–CuO nanomaterials with enhanced catalytic potential," *Ceramics International*, vol. 50, no. 20, Part B, p. 39262-39277, 2024.

https://doi.org/10.1016/j.ceramint.2024.07.297.

[26] L. Anju Chanu, W. Joychandra Singh, K. Jugeshwar Singh, and K. Nomita Devi, "Effect of operational parameters on the photocatalytic degradation of Methylene blue dye solution using manganese doped ZnO nanoparticles," *Results in Physics*, vol. 12, p. 1230-1237, 2019.

https://doi.org/10.1016/j.rinp.2018.12.089.

[27] M. Nasrollahzadeh, M. Sajjadi, M. Maham, S. M. Sajadi, and A. A. Barzinjy, "Biosynthesis of the palladium/sodium borosilicate nanocomposite using Euphorbia milii extract and evaluation of its catalytic activity in the reduction of chromium(VI), nitro compounds and organic dyes," *Materials Research Bulletin*, vol. 102, p. 24-35, 2018.

https://doi.org/10.1016/j.materresbull.2018.01.032.

[28] T. Li *et al.*, "General self-assembly of metal/metal chalcogenide heterostructures initiated by a surface linker: modulating tunable charge flow toward versatile photoredox catalysis," *Journal of Materials Chemistry A*, 10.1039/C9TA07569K vol. 7, no. 37, p. 21182-21194, 2019.

https://doi.org/10.1039/C9TA07569K.

[29] M. Sankar, M. Jothibas, A. Muthuvel, A. Rajeshwari, and S. J. Jeyakumar, "Structural, optical and Photocatalytic degradation of organic dyes by sol gel prepared Ni doped CdS nanoparticles," *Surfaces and Interfaces*, vol. 21, p. 100775, 2020.

https://doi.org/10.1016/j.surfin.2020.100775.

[30] J.-M. Herrmann, "Heterogeneous photocatalysis: fundamentals and applications to the removal of various types of aqueous pollutants," *Catalysis Today*, vol. 53, no. 1, p. 115-129, 1999.

https://doi.org/10.1016/S0920-5861(99)00107-8.

[31] S. Yousaf *et al.*, "Solar light irradiated photocatalytic activity of ZnO–NiO/rGO nanocatalyst," *Journal of Materials Research and Technology*, vol. 12, p. 999-1009, 2021.

https://doi.org/10.1016/j.jmrt.2021.03.012.

[32] L. Ma *et al.*, "Improved Photocatalytic Activity via n-Type ZnO/p-Type NiO Heterojunctions," *Nanomaterials*, vol. 12, no. 20,

https://doi.org/10.3390/nano12203665